Nonadiabatic Molecular Quantum Dynamics with Quantum Computers

Pauline J. Ollitrault,[1,2] Guglielmo Mazzola,[1] and Ivano Tavernelli[1]
[1]IBM Quantum, IBM Research–Zurich, Säumerstrasse 4, 8803 Rüschlikon, Switzerland
[2]Laboratory of Physical Chemistry, ETH Zurich, Vladimir-Prelog-Weg 2, 8093 Zurich, Switzerland

(Received 16 June 2020; accepted 10 December 2020; published 31 December 2020)

The theoretical investigation of nonadiabatic processes is hampered by the complexity of the coupled electron-nuclear dynamics beyond the Born-Oppenheimer approximation. Classically, the simulation of such reactions is limited by the unfavorable scaling of the computational resources as a function of the system size. While quantum computing exhibits proven quantum advantage for the simulation of real-time dynamics, the study of quantum algorithms for the description of nonadiabatic phenomena is still unexplored. In this Letter, we propose a quantum algorithm for the simulation of fast nonadiabatic chemical processes together with an initialization scheme for quantum hardware calculations. In particular, we introduce a first-quantization method for the time evolution of a wave packet on two coupled harmonic potential energy surfaces (Marcus model). In our approach, the computational resources scale polynomially in the system dimensions, opening up new avenues for the study of photophysical processes that are classically intractable.

DOI: 10.1103/PhysRevLett.125.260511

Fast nonadiabatic processes are ubiquitous in science as they are the foundation of photoinduced reactions spanning the fields of biology [1–5], chemical engineering, and material science [6,7]. From an atomistic standpoint, nonadiabatic dynamics account for various interesting phenomena. These include internal conversion and intersystem crossings among Born-Oppenheimer (BO) potential energy surfaces (PESs), the Jahn-Teller effect [8], and vibrational assisted energy versus electron transfer [9–11].

In molecular systems, nonadiabatic processes occur through the dynamical coupling between the electronic and vibrational nuclear degrees of freedom. They are characterized by the breakdown of the BO approximation [12]. However, the simultaneous description of the dynamics of the electronic and nuclear wave functions poses severe limitations to the size of the systems that can be simulated and to the accuracy of the solutions. From a theoretical standpoint, relentless efforts have been made to refine numerical methods to simulate nonadiabatic phenomena beyond the analytically solvable Landau-Zener model [13]. First numerical attempts evolved around a semiclassical solution of the problem, e.g., within the Wenzel-Kramers-Brillouin approximation [14], the Ehrenfest dynamics [15], and trajectory surface hopping [16]. These approaches have been extended to the study of nonadiabatic effects in molecules and solid state systems using first principle electronic structure approaches for the BO PESs [10,17]. However, the use of classical and quantum trajectories hampers a correct description of quantum phenomena, such as wave packet branching at avoided crossings, tunneling, and quantum coherence and decoherence effects.

More naturally, the quantum dynamics of the nuclear wave function can be represented as a wave packet, especially in those regimes where dynamics cannot be faithfully described by classical, semiclassical or quantum trajectories [18]. To this end, the direct solution of the time-dependent Schrödinger equation for the nuclear degrees of freedom is required. However, due to the exponential scaling of the Hilbert space, grid methods can only be applied to low-dimensional model Hamiltonians while the use of basis functions is usually limited to a few nuclear degrees of freedom [19–21].

State-of-the-art approaches, like the multiconfiguration time-dependent Hartree (MCTDH) method [22,23], can routinely tackle up to ten dimensions [24,25], but not without the use of approximations. In fact, as MCTDH relies on a compact time-dependent basis set description, the integration becomes less accurate as the propagation time increases, or when the dynamics becomes chaotic. Further approximations have been introduced with the aim at improving the efficiency of the method. These include nonorthogonal Gaussian-based GMCTDH [26], local coherent state approximation [27], and multiple spawning [28].

Quantum computers can in principle simulate real-time quantum dynamics with polynomial complexity in memory and execution time. Indeed, the simulation of quantum physics with quantum computers has been proposed theoretically decades ago by Feynman [29], and realized experimentally in the last years for electronic structure calculations [30–37]. Of particular interest is the possibility to perform wave packet dynamics simulations in real-space representation [38,39] with a quantum computer. Within this framework, the space is discretized in a mesh of $\mathcal{N}$

points, separated by a distance Δx, in each dimension, that requires order $\log_2(\mathcal{N})$ memory space in the quantum register. The accuracy of the dynamics is not bounded by any basis set limitation but rather by Δx. A general procedure for the real-time propagation of a quantum state on a quantum computer was first introduced by Kassal *et al.* [40]. However, this work did not specify how to encode the potential and kinetic energy terms of the time evolution operator into a quantum circuit (i.e., into operations on the qubits). Benenti and Strini [41] and later Somma [42] presented a more detailed implementation in the case of a single, one-dimensional, harmonic potential. Additionally, a quantum circuit to implement a spin-boson model has also been devised in Ref. [43]. In this case, the dynamical bosonic degrees of freedom in the model are represented as a wave packet evolving under the action of a harmonic oscillator Hamiltonian, where the displacement operators are coupled with the σ^z operator(s) of the spin(s). Finally, a different approach consists of encoding the bosonic modes directly in the hardware, exploiting the microwave resonators available in the device [44,45].

In this Letter, we devise a quantum algorithm for the simulation of nonadiabatic processes using a real-space representation of the wave packet. While described in a one-dimensional case, the method can easily be extended to the study of the quantum dynamics of larger systems by implementing additional spatial dimensions in the qubit register. The scheme is applied to the investigation of the dynamics of the one-dimensional Marcus model defined by two coupled harmonic potential energy curves, for which we observe the characteristic modulation of the charge transfer rates when going from the *normal* to the so-called *inverted* Marcus regime [46]. Finally, we discuss and demonstrate the initialization of the Gaussian wave packet on a quantum register.

The model.—The method aims at studying the dynamics of a wave packet in several diabatic surfaces coupled through nonlinear matrix elements in the first quantization formalism. For the sake of simplicity here we restrict the model to two one-dimensional diabatic curves. Note, however, that the generalization to multiple dimensions is straightforward.

The Hamiltonian of the system can then be written as

$$H = K \otimes \mathbb{1} + V_0 \otimes |0\rangle\langle 0| + V_1 \otimes |1\rangle\langle 1| + C \otimes \sigma_x, \quad (1)$$

where $K = 1/2mp^2$ is the kinetic energy operator of a particle with mass m, while V_0 and V_1 are the potentials of the first and the second diabatic curves, respectively, and are defined by functions of the position x. Likewise, the coupling operator C is described by an arbitrary function of the position $f(x)$. An ancilla qubit q_N, is entangled with the spacial register and controls the nonadiabatic dynamics across the diabatic curves. It is initialized in state $|0\rangle$ ($|1\rangle$) if the wave packet at time $t = 0$ is placed on the first (second) diabatic potential V_0 (V_1). For concreteness we specialize to the Marcus model [46,47] which provides a simplified description of the electron-transfer reaction rate driven by collective outer and inner sphere coordinates [48]. In this model, the potentials of Eq. (1) are defined by $V_i = \omega_i^2/2m(x - x_i^0)^2 + \Delta_r G_i^0$. The two harmonic potentials of the diabatic curves differ by an energy shift $\Delta_r G_i^0$, frequency ω_i, equilibrium position x_i^0, and model the reactant and product states, respectively. We call *offset* the difference $\Delta_r G_1^0 - \Delta_r G_0^0$. We use this setup in what follows and show its representation in Fig. 1(a).

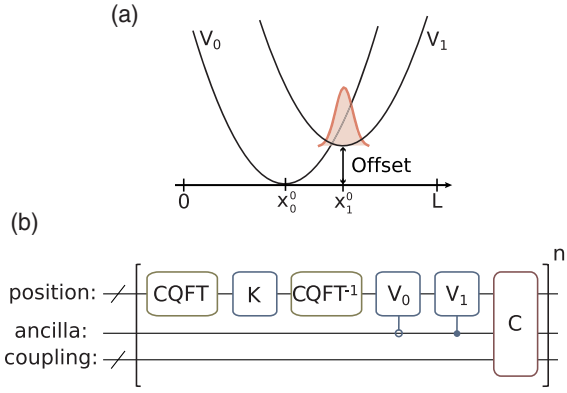

FIG. 1. (a) Graphical representation of the Marcus model. (b) Circuit for the time evolution of the wave packet. The K, V_i, and C blocks represent the time evolution operators for the kinetic, ith potential and coupling terms, respectively.

Resources scaling.—The position is encoded in the qubit register as $x = j \times \Delta x$ where j is an integer which binary representation is encoded in the basis states of $N = \log_2(\mathcal{N})$ qubits. Thus, in general, we require $d\log_2(\mathcal{N})$ qubits to store the total wave function of the wave packet in d dimensions. An ancillary register of size $\lceil \log_2(\kappa) \rceil$ is needed to describe dynamics involving up to κ diabatic potential energy surfaces. In the specific model considered here, we only need one ancillary qubit for the propagation of the wave packet in V_0 and V_1 coupled through the nonadiabatic coupling operator C. Additionally, an extra qubit register is required to implement C which size depends linearly on N as well as on the shape of the coupling as explained later and in the Supplemental Material [49].

The time-evolution algorithm.—The very first step of the dynamics resides in the initialization of the wave packet in the quantum register. In the interest of clarity, this step will be discussed in further detail at the end of this Letter and in the Supplemental Material [49]. Then the wave packet is propagated under the action of the real-time evolution operator such that $|\Psi(t)\rangle = e^{-(i/\hbar)Ht}|\Psi(t=0)\rangle$, using the Lie-Trotter-Suzuki product formulas [53]. A quantum circuit for implementing the time evolution under the kinetic operator and harmonic potentials was presented in Refs. [41,42] and is detailed in the Supplemental

Material [49]. The same logic can be extended to potentials described by a polynomial function of the position. Note that to account for negative values of the momentum, a shift of $p_c = \Delta p \mathcal{N}/2$, where $\Delta p = 2\pi/\mathcal{N}\Delta x$, is applied placing the zero momentum value at the center of the Brillouin zone. This choice implies the use of a centered quantum Fourier transform (CQFT) operator (see Supplemental Material for details [49]) to implement the switch from the position to the momentum space. While the quantum circuit for the kinetic part of the evolution can directly be applied on the first N qubits, the potential parts must be controlled by the state of the ancilla qubit q_N, such that the wave packet evolves under the action of $e^{-iV_0 t/n}$ and $e^{-iV_1 t/n}$ when q_N is in the $|0\rangle$ and $|1\rangle$ state, respectively (here n is the number of Trotter steps).

One of the main methodological novelties of this work resides in the encoding of the coupling operator which acts as

$$e^{-iC\otimes\sigma_x t/n}|x\rangle|q_N\rangle = e^{-if(x)\sigma_x t/n}|x\rangle|q_N\rangle \tag{2}$$

and thus corresponds to a rotation of the ancilla qubit around the x axis by an angle $f(x)t/n$. The general approach consists in precomputing a discretized function $f(x)$ into additional qubits using quantum arithmetic. While the number of gates and the number of additional qubits scale exponentially with the inverse desired accuracy for a general function [54], the resources can be kept reasonably low by approximating $f(x)$ as a piecewise linear function [55]. In the approach adopted here, the additional gates and ancilla qubits scale linearly with N and with the number of pieces in the description of $f(x)$ (see Supplemental Material [49] and Refs. [56,57]). The generalization to multiple surfaces is also possible keeping the scaling invariant as discussed in the Supplemental Material [49]. Crucially, we observe that accurate results can be obtained by including only a few pieces in $f(x)$. A graphical representation of the quantum circuit used to encode the dynamics is shown in Fig. 1(b). We expect the approximation of the coupling function to have a larger impact on the accuracy of the dynamics when the adiabaticity [58] is weak. This is the case when the offset [Fig. 1(a)] approaches the reorganization energy (see the Supplemental Material [49]).

Rates in the Marcus model.—The model parameters are chosen to represent typical molecular dynamics [59] and the simulation conditions were optimized to guarantee the convergence of the results (see the Supplemental Material [49]).

Therefore, we choose to discretize a space of length $L = 20$ using 8 qubits and we select a time step of 10 a.u. The nonadiabatic coupling term, which in the reference model is a Gaussian function, is approximated with a step function giving the best trade-off between accuracy and number of additional qubits that, in this case, amounts to 9 qubits. The time evolution is performed for a total time of

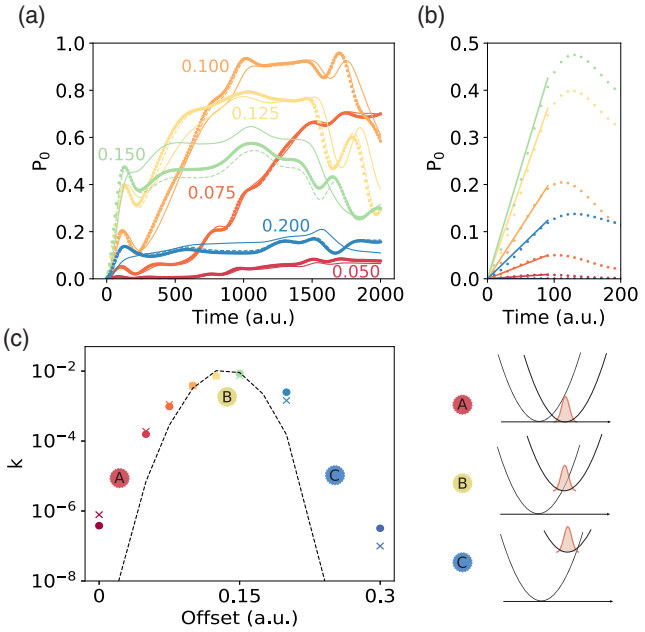

FIG. 2. (a) Time evolution of P_0 (see main text) obtained with our algorithm in classical simulations (dots), with the exact evolution with the reference coupling (full lines) and with the exact evolution with the approximate coupling (dashed lines). Curves at different offset values are displayed. (b) Linear fitting of the ten first steps of the evolution to approximate the rate constant. (c) The approximated rate constant k as a function of the offset obtained with our algorithm (dots) and with the exact evolution with the reference coupling (crosses). The Marcus rates as calculated in the Supplemental Material [49] are shown in dashed line for a qualitative comparison. The colored stickers label the different charge transfer regions (A, normal regime; B, at reorganization energy; and C, inverted region).

$T = 2000$ a.u. and repeated for different values of the offset between the two harmonic potential energy curves.

For the time being, we assume a Gaussian state preparation of the form (see below) [59]

$$\phi_0(x) = \left(\frac{1}{2\pi\delta^2}\right)^{1/4} e^{-[(x-x_0)/2\delta]^2} e^{ip_0(x-x_0)}, \tag{3}$$

at the center of the potential curve at the right, V_1, at $x_0 = 11.5$ [see Fig. 1(a)] with $\delta = 1/3$. The initial momentum is set to $p_0 = 1$. This choice is motivated from the possibility to compare with the standard Marcus rate theory (see Supplemental Material [49]). Note, however, that the qualitative behavior of the dynamics is not affected by the particular value of p_0.

At each time step, the population fraction P_0 in the product well V_0, is simply related to the expectation value of the ancilla qubit as $P_0 = (\langle Z_{q_N}\rangle + 1)/2$ (where Z is the Pauli operator σ_z). We run the dynamics for various offset values and show the time evolution of corresponding P_0 in Fig. 2(a) (dots), using a classical emulation of the

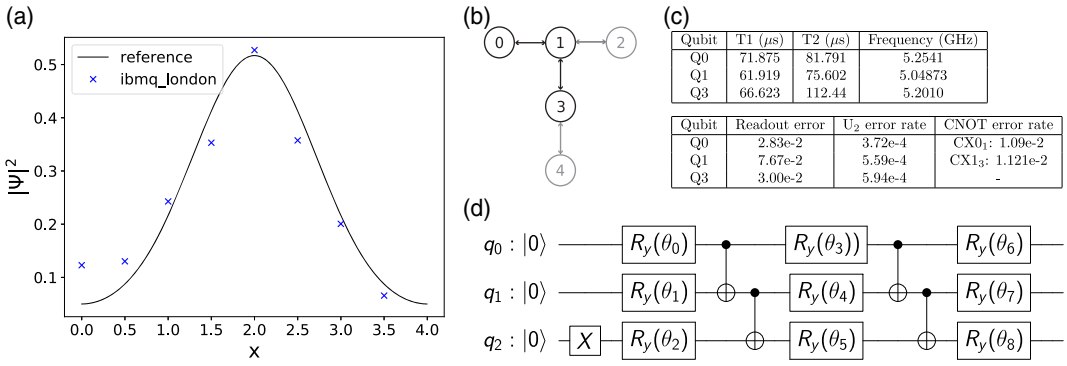

Qubit	T1 (μs)	T2 (μs)	Frequency (GHz)
Q0	71.875	81.791	5.2541
Q1	61.919	75.602	5.04873
Q3	66.623	112.44	5.2010

Qubit	Readout error	U_2 error rate	CNOT error rate
Q0	2.83e-2	3.72e-4	$CX0_1$: 1.09e-2
Q1	7.67e-2	5.59e-4	$CX1_3$: 1.121e-2
Q3	3.00e-2	5.94e-4	-

FIG. 3. (a) Initialization of a wave packet in the *ibmq_london* 5-qubit device. The quantum circuit representing the discretized version of the reference wave packet (black curve) is obtained from a classical simulation of the VQE algorithm. (b) Layout of the *ibmq_london* quantum computer. The qubits in black are the ones used to prepare the wave packet. (c) Specifications of the qubit used to prepare the wave packet. (d) Quantum circuit for the preparation of the wave packet. The values of the optimized angles are $\theta_0 = -0.3383$, $\theta_1 = -1.5502$, $\theta_2 = 2.3662$, $\theta_3 = -0.6743$, $\theta_4 = -0.5438$, $\theta_5 = -2.0766$, $\theta_6 = -1.3717$, $\theta_7 = 0.3663$, $\theta_8 = -0.8286$.

corresponding quantum circuit. The exact evolution obtained with the original, Gaussian, coupling (full lines) and with its piecewise approximation (dashed lines) is also reported demonstrating the correct implementation of the algorithm (the small discrepancies are due to Trotter errors). Moreover, these results highlight that the piecewise linear approximation of the coupling function allows us to recover the correct qualitative quantum dynamics. Note that the accuracy of the results is controllable as it can be systematically increased by improving the representation of the coupling function, as well as by reducing the Trotter step. We calculate the initial rate constant k for each offset by taking the slope of the linear fit applied to the first ten steps of the dynamics as shown in Fig. 2(b). The rates obtained from the quantum dynamics (dots) and from the exact dynamics with the exact, Gaussian, coupling (crosses) are in good agreement and are summarized in Fig. 2(c). As expected, the population transfer rate increases with the offset in the normal Marcus regime, reaching a maximum value when the offset is equal to the reorganization energy before decreasing again in the inverted region, thus recovering the expected volcano shape predicted by Marcus theory [dashed line in Fig. 2(c)]. Note that discrepancies between the Marcus rates, calculated for a carefully chosen effective temperature (see Supplemental Material [49]) and our rate estimates are expected, as we are performing a closed-system dynamics.

Initial state preparation.—To complete our presentation, we discuss an equally efficient initial state preparation method. To this end, we rely on a more efficient variational quantum eigensolver (VQE) [60–63] approach instead of quantum arithmetic based methods [64,65]. As a proof of concept we show how to prepare a wave packet defined as the ground state of the (arbitrarily chosen) Hamiltonian defined on a 3-qubit register (see Supplemental Material for the detail [49]). The parametrized circuit comprises three layers of R_y rotations intersected of three layers of CNOT gates as shown in Fig. 3(d). In the Supplemental Material [49] we study the convergence of the VQE in presence of noise with the state-of-the-art optimizer and show that it requires an important number of optimization steps as well as error mitigation. Here, the circuit can be optimized in a fully classical simulation of the VQE algorithm. We employ this circuit on three qubits of the *ibmq_london* 5-qubit chip [see the hardware layout and the qubits specifications in Figs. 3(b) and 3(c) respectively]. Since in this example $p_0 = 0$ (i.e., the wave function is real) we simply display the modulo squared of the resulting wave function (obtained by measuring 8000 times in the position basis) in Fig. 3(a). We also show the reference Gaussian function demonstrating the initialization of the desired wave packet in the quantum computer.

Conclusion.—We introduced a quantum algorithm to simulate the propagation of a nuclear wave packet across κ diabatic surfaces, featuring nonlinear couplings. The degrees of freedom are expressed in the first quantization formalism, as the position and momentum spaces are discretized and encoded in a *position* quantum register. Ancilla registers are used to encode the real-time evolution of the population transfer between the κ surfaces, and to realize the nonlinear coupling operators. The encoding of the problem is efficient in term of qubit resources, which scale logarithmically with the precision. This impressive memory compression in storing the time-evolved wave function, represented in a systematically converging basis set of a real-space $\mathcal{N}$-point grid, readily realizes an exponential quantum advantage compared to classical algorithms. As discussed, the proposed circuit to perform the coupled-time evolution only requires a polynomially scaling depth. We demonstrate this approach to simulate the nonadiabatic dynamics of a wave packet evolving in a Marcus model, consisting in two one-dimensional harmonic potentials shifted in energy by a variable offset. This minimal model requires a feasible number of qubits (eighteen), so that the circuit can be classically emulated. The simulated dynamics are in excellent agreement with

the exact propagation and we are able to observe the expected slowing down of the population transfer in the so-called *inverted region*. However, the circuit depth required to observe these dynamics greatly exceeds those currently feasible due to the limited coherence time of present quantum hardware. Therefore, we limit the hardware demonstration to the first part of the algorithm, i.e., the Gaussian wave packet initialization, on an IBM Q device.

As far as concerning the quantum resources (number of qubits), our algorithm can straightforwardly be extended to represent polynomial potential energy surfaces in d dimensions with a scaling $\mathcal{O}(d\log_2(\mathcal{N}))$. Hence, a quantum computer with ∼165 qubits would allow for the study of molecular systems characterized by up to ten vibrational modes. Reaching the limits of classical simulations [66,67], this approach will pave the way toward a better understanding of femtochemistry processes, such as internal conversion and intersystem crossings, exciton formation, and charge separation.

The authors thank Julien Gacon, Almudena Carrera Vazquez, and Stefan Woerner for useful discussions and acknowledge financial support from the Swiss National Science Foundation (SNF) through Grant No. 200021-179312.

[1] W. Domcke and G. Stock, *Advances in Chemical Physics* (Wiley, New York, 1997), https://www.wiley.com/en-sg/Advances+in+Chemical+Physics,+Volume+100-p-9780470141595.
[2] G. A. Worth and L. S. Cederbaum, Annu. Rev. Phys. Chem. **55**, 127 (2004).
[3] W. Domcke and D. R. Yarkony, Annu. Rev. Phys. Chem. **63**, 325 (2012).
[4] M. S. Schuurman and A. Stolow, Annu. Rev. Phys. Chem. **69**, 427 (2018).
[5] D. R. Yarkony, J. Phys. Chem. A **105**, 6277 (2001).
[6] A. Hagfeldt and M. Graetzel, Chem. Rev. **95**, 49 (1995).
[7] C. W. Tang and S. A. Vanslyke, Appl. Phys. Lett. **51**, 913 (1987).
[8] I. Bersuker, *The Jahn-Teller Effect and Vibronic Interactions in Modern Chemistry* (Springer Science & Business Media, New York, 2013), https://link.springer.com/book/10.1007%2F978-1-4613-2653-3.
[9] T. Nelson, A. White, J. Bjorgaard, A. Sifain, Y. Zhang, B. Nebgen, S. Fernandez-Alberti, D. Mozyrsky, A. Roitberg, and S. Tretiak, Chem. Rev. **120**, 2215 (2020).
[10] I. Tavernelli, Acc. Chem. Res. **48**, 792 (2015).
[11] S. J. Jang and B. Mennucci, Rev. Mod. Phys. **90**, 035003 (2018).
[12] G. A. Worth and L. S. Cederbaum, Annu. Rev. Phys. Chem. **55**, 127 (2004).
[13] C. Zener, Proc. R. Soc. A **137**, 696 (1932).
[14] W. H. Miller, J. Chem. Phys **53**, 3578 (1970).
[15] P. Ehrenfest, Z. Phys. **45**, 455 (1927).
[16] J. C. Tully, J. Chem. Phys. **93**, 1061 (1990).
[17] B. F. E. Curchod and T. J. Martínez, Chem. Rev. **118**, 3305 (2018).
[18] X. Sun and W. H. Miller, J. Chem. Phys. **106**, 6346 (1997).
[19] R. Kosloff, Annu. Rev. Phys. Chem. **45**, 145 (1994).
[20] B. M. Garraway and K.-A. Suominen, Rep. Prog. Phys. **58**, 365 (1995).
[21] J. Huang, S. Liu, D. H. Zhang, and R. V. Krems, Phys. Rev. Lett. **120**, 143401 (2018).
[22] H.-D. Meyer, U. Manthe, and L. S. Cederbaum, Chem. Phys. Lett. **165**, 73 (1990).
[23] M. H. Beck, A. Jäckle, G. A. Worth, and H.-D. Meyer, Phys. Rep. **324**, 1 (2000).
[24] D. Egorova, A. Kühl, and W. Domcke, Chem. Phys. **268**, 105 (2001).
[25] H.-D. Meyer and G. A. Worth, Theor. Chem. Acc. **109**, 251 (2003).
[26] I. Burghardt, K. Giri, and Worth, J. Chem. Phys. **129**, 174104 (2008).
[27] R. Martinazzo, M. Nest, P. Saalfrank, and G. F. Tantardini, J. Chem. Phys. **125**, 194102 (2006).
[28] T. J. Martínez and R. D. Levine, J. Chem. Soc., Faraday Trans. **93**, 941 (1997).
[29] R. P. Feynman, Int. J. Theor. Phys. **21**, 467 (1982).
[30] A. Kandala, A. Mezzacapo, K. Temme, M. Takita, M. Brink, J. M. Chow, and J. M. Gambetta, Nature (London) **549**, 242 (2017).
[31] J. I. Colless, V. V. Ramasesh, D. Dahlen, M. S. Blok, M. E. Kimchi-Schwartz, J. R. McClean, J. Carter, W. A. de Jong, and I. Siddiqi, Phys. Rev. X **8**, 011021 (2018).
[32] A. Kandala, K. Temme, A. D. Córcoles, A. Mezzacapo, J. M. Chow, and J. M. Gambetta, Nature (London) **567**, 491 (2019).
[33] Y. Nam, J.-S. Chen, N. C. Pisenti, K. Wright, C. Delaney, D. Maslov, K. R. Brown, S. Allen, J. M. Amini, J. Apisdorf *et al.*, arXiv:1902.10171.
[34] P. J. Ollitrault, A. Kandala, C.-F. Chen, P. K. Barkoutsos, A. Mezzacapo, M. Pistoia, S. Sheldon, S. Woerner, J. M. Gambetta, and I. Tavernelli, Phys. Rev. Research **2**, 043140 (2020).
[35] P. J. J. O'Malley, R. Babbush, I. D. Kivlichan, J. Romero, J. R. McClean, R. Barends, J. Kelly, P. Roushan, A. Tranter, N. Ding *et al.*, Phys. Rev. X **6**, 031007 (2016).
[36] C. Hempel, C. Maier, J. Romero, J. McClean, T. Monz, H. Shen, P. Jurcevic, B. P. Lanyon, P. Love, R. Babbush *et al.*, Phys. Rev. X **8**, 031022 (2018).
[37] S. Paesani, A. A. Gentile, R. Santagati, J. Wang, N. Wiebe, D. P. Tew, J. L. O'Brien, and M. G. Thompson, Phys. Rev. Lett. **118**, 100503 (2017).
[38] C. Zalka, Proc. R. Soc. A **454**, 313 (1998).
[39] S. Wiesner, arXiv:quant-ph/9603028.
[40] I. Kassal, S. P. Jordan, P. J. Love, M. Mohseni, and A. Aspuru-Guzik, Proc. Natl. Acad. Sci. U.S.A. **105**, 18681 (2008).
[41] G. Benenti and G. Strini, Am. J. Phys. **76**, 657 (2008).
[42] R. D. Somma, arXiv:1503.06319v2.
[43] A. Macridin, P. Spentzouris, J. Amundson, and R. Harnik, Phys. Rev. Lett. **121**, 110504 (2018).
[44] D. Ballester, G. Romero, J. J. García-Ripoll, F. Deppe, and E. Solano, Phys. Rev. X **2**, 021007 (2012).

[45] J. Leppäkangas, J. Braumüller, M. Hauck, J.-M. Reiner, I. Schwenk, S. Zanker, L. Fritz, A. V. Ustinov, M. Weides, and M. Marthaler, Phys. Rev. A **97**, 052321 (2018).
[46] R. A. Marcus, Rev. Mod. Phys. **65**, 599 (1993).
[47] R. A. Marcus, Annu. Rev. Phys. Chem. **15**, 155 (1964).
[48] P. Siders and R. A. Marcus, J. Am. Chem. Soc. **103**, 748 (1981).
[49] See Supplemental Material at http://link.aps.org/supplemental/10.1103/PhysRevLett.125.260511 for details on the optimization procedure, which include Refs. [50–52].
[50] J. C. Spall, IEEE Trans. Autom. Control **45**, 1839 (2000).
[51] R. A. Marcus, J. Chem. Phys. **24**, 966 (1956).
[52] A. Nitzan, *Chemical Dynamics in Condensed Phases: Relaxation, Transfer and Reactions in Condensed Molecular Systems* (Oxford University Press, New York, 2006).
[53] D. W. Berry, G. Ahokas, R. Cleve, and B. C. Sanders, Commun. Math. Phys. **270**, 359 (2007).
[54] K. Mitarai, M. Kitagawa, and K. Fujii, Phys. Rev. A **99**, 012301 (2019).
[55] T. Häner, M. Roetteler, and K. M. Svore, arXiv:1805.12445.
[56] S. Woerner and D. J. Egger, npj Quantum Inf. **5**, 15 (2019).
[57] N. Stamatopoulos, D. J. Egger, Y. Sun, C. Zoufal, R. Iten, N. Shen, and S. Woerner, Quantum **4**, 291 (2020).
[58] M. P. Bircher, E. Liberatore, N. J. Browning, S. Brickel, C. Hofmann, A. Patoz, O. T. Unke, T. Zimmermann, M. Chergui, P. Hamm *et al.*, Struct. Dyn. **4**, 061510 (2017).
[59] T. Yonehara and K. Takatsuka, J. Chem. Phys. **132**, 244102 (2010).
[60] A. Peruzzo, J. McClean, P. Shadbolt, M.-H. Yung, X.-Q. Zhou, P. J. Love, A. Aspuru-Guzik, and J. L. O'Brien, Nat. Commun. **5** (2014).
[61] M.-H. Yung, J. Casanova, A. Mezzacapo, J. Mcclean, L. Lamata, A. Aspuru-Guzik, and E. Solano, Sci. Rep. **4**, 3589 (2014).
[62] J. R. McClean, J. Romero, R. Babbush, and A. Aspuru-Guzik, New J. Phys. **18**, 023023 (2016).
[63] D. Wang, O. Higgott, and S. Brierley, Phys. Rev. Lett. **122**, 140504 (2019).
[64] L. Grover and T. Rudolph, arXiv:quant-ph/0208112.
[65] A. Kitaev and W. A. Webb, arXiv:0801.0342.
[66] G. Capano, M. Chergui, U. Rothlisberger, I. Tavernelli, and T. J. Penfold, J. Phys. Chem. A **118**, 9861 (2014).
[67] A. Zhugayevych and S. Tretiak, Annu. Rev. Phys. Chem. **66**, 305 (2015).